Quantum Correlations in Engineered Magneto-Sensitive Fluorescent Proteins Enables Multi-Modal Sensing in Living Cells

Gabriel Abrahams[1*], Vincent Spreng[1,2†], Ana Štuhec[3†], Idris Kempf[1], Jessica James[1], Kirill Sechkar[1], Scott Stacey[1], Vicente Trelles-Fernandez[1], Lewis M. Antill[3,4], Maria Ingaramo[5], Andrew York[5], Jean-Philippe Tetienne[6], Christiane R. Timmel[3], Harrison Steel[1*]

[1*]Department of Engineering, University of Oxford, Parks Road, Oxford, OX14PJ, Oxfordshire, United Kingdom.
[2] Faculty of Engineering Sciences, Heidelberg University, Heidelberg, Germany .
[3]Department of Chemistry, University of Oxford, Chemistry Research Laboratory, 12 Mansfield Road, Oxford, OX1 3TA, Oxfordshire, United Kingdom.
[4]Institute of Quantum Biophysics, Department of Biophysics, Sungkyunkwan University, Suwon, 16419, Republic of Korea.
[5]Calico Life Sciences, 1170 Veterans Blvd, South San Francisco, 94080, California, United States.
[6]School of Science, RMIT University, Melbourne, VIC 3001, Australia.

*Corresponding author(s). E-mail(s): gabriel.abrahams@eng.ox.ac.uk; harrison.steel@eng.ox.ac.uk;
†These authors contributed equally to this work.

Abstract

Quantum mechanical phenomena have been identified as fundamentally significant to an increasing number of biological processes. Simultaneously, quantum sensing is emerging as a cutting-edge technology for precision biosensing. However, biological based candidates for quantum-sensors have thus far been limited to *in vitro* systems, are prone to light induced degradation, and require

sophisticated experimental setups making high-throughput studies prohibitively complex. We recently created a new class of magneto-sensitive fluorescent proteins (MFPs) [1], which we now show overcome these challenges and represent the first biological quantum-based sensor that functions at physiological conditions and in living cells. Through directed evolution, we demonstrate the possibility of engineering these proteins to alter properties of their response to magnetic fields and radio frequencies. These effects are explained in terms of the spin correlated radical pair (SCRP) mechanism, involving the protein backbone and a bound flavin cofactor. Using this engineered system we demonstrate the first observation of a fluorescent protein exhibiting Optically Detected Magnetic Resonance (ODMR) in living bacterial cells at room temperature, at sufficiently high signal-to-noise to be detected in a single cell, paving the way for development of a new class of *in vivo* biosensors. We further demonstrate the use of multiple variants of MFPs for multiplexing or lock-in amplification of fluorescence signals, opening a new approach to combining or extracting multiple signals from a biological measurement. Taken together, our results represent a new intersection of imaging and perhaps actuation modalities for engineered biological systems, based on and designed around understanding the quantum mechanical properties of MFPs.

Keywords: Biosensing, Quantum, ODMR, ESR, RYDMR, Magnetic Field Effects, Quantum Sensing

1 Introduction

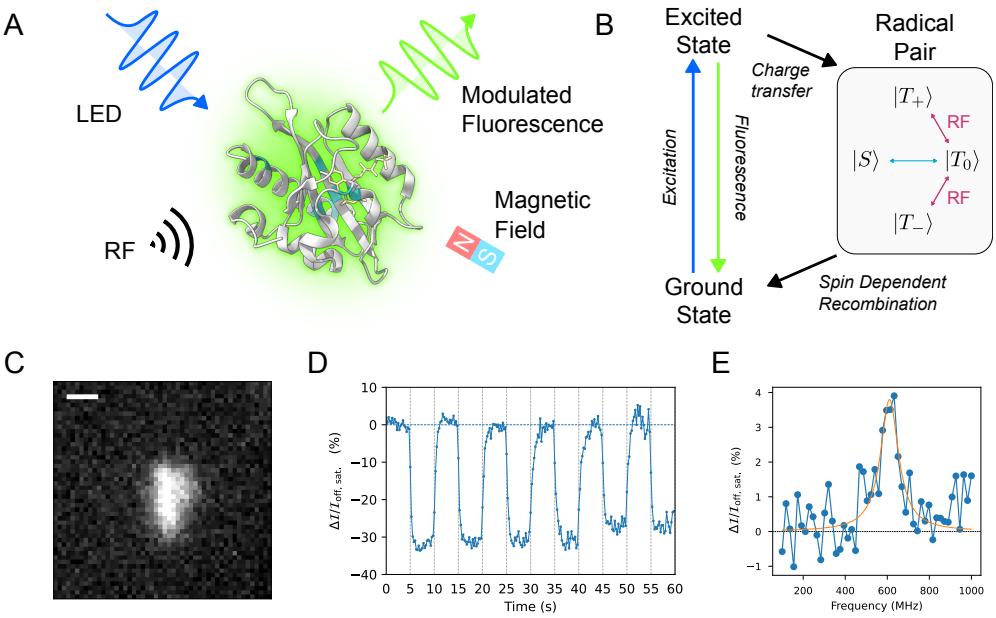

Fig. 1 Principles of magneto-sensitive fluorescent proteins. A. Structure of AsLOV2 PDB 2V1A[2] with mutations resutling in MagLOV 2 highlighted. For the first time, quantum sensing in living cells using a fluorescent protein-based sensor can be performed by driving spin transitions using radio-frequency (RF) fields in the presence of a static magnetic field. **B.** Simplified photocycle diagram in the case of a large external magnetic field. The eigenstates in the strong coupling regime (spin coupling $\gg$ hyperfine coupling) are the singlet ($S = 0$) state $|S\rangle$, and triplet ($S = 1$) states with three available spin projections $|T_0\rangle$, $|T_+\rangle$ and $|T_-\rangle$[3, 4]. **C.** Microscope image cropped to a single cell expressing MagLOV 2 R11 f. Scalebar is 1 µm. **D.** For MFE measurements the magnetic field was modulated between 0 mT and 10 mT, here with a period of 10 s. The intensity over time is integrated over pixels covering the single cell (here expressing MagLOV 2 R11 f), with an exponential decay (due to photobleaching) removed. **E.** A single cell expressing MagLOV 2 R11 f displaying an ODMR signal with 4 % contrast.

Coupling electromagnetic fields with biological processes through fluorescence has revolutionised quantitative biology [5, 6]. However, the application of quantum mechanical phenomena have thus far been restricted to non-biological probes [7, 8] or measurements under *ex vivo* conditions [9–11]. We recently developed a library of magneto-responsive fluorescent protein (MFP) variants derived from the LOV2 domain, which exhibit fluorescence signals with large magnetic field effects (MFEs) arising from quantum spin dependent processes [1] [Fig. 1 A-D]. In this work, we present a new finding, that living cells expressing these proteins exhibit optically detected magnetic resonance (ODMR) in their fluorescence, at room temperature (Section 2), and detectable in single cells [Fig. 1 E]. The ODMR signature implies a quantum system whose properties and dynamics sensitively depend on the local

environment, opening up a broad range of novel possibilities for cellular biosensing [7]. The ODMR arises from an electron spin resonance (ESR) that we hypothesise originates from a spin correlated radical pair (SCRP) [Fig. 1 B] involving the LOV2 domain non-covalently bound flavin co-factor chromophore. This theory is based on prior evidence [12] and supported by the MFE, ODMR and spectral data presented here (Section 3).

Importantly for adoption, both MFE and ODMR signals are straightforward to detect in cells on a standard wide-field fluorescence microscope, a promising start for further experimental platform development. Besides the ease of detecting MFP's magnetic resonance via fluorescence emission, MFPs are advantageous over other candidate spin labels for biological uses because they can be expressed directly in the host organism (e.g. in a regulated way) and because their performance can be engineered genetically, such as through rational design or directed evolution. This engineerability is demonstrated through the selection approach previously reported[1] and here used to generate two novel variants MagLOV 2 and MagLOV 2 R11 f, selecting for improved MFEs.

Furthermore, we demonstrate applications of MFPs as fluorescent reporters that can be used for lock-in signal amplification in noisy signal environments, and to enable signal multiplexing by engineering variants with differing dynamic responses (Sections 4 and 5). The realisation of ODMR imaging broadens the application space significantly. For example, as the resonance condition depends on the static magnetic field at the location of the protein, we envisage the use of gradient fields as in magnetic resonance imaging to enable a 3D spatially localised protein reporter. Furthermore, the possibility of controlling charge state transfers at the protein raises the possibility of developing 3D spatially localised optogenetic actuators e.g. by coupling to a conformation switchable domain.

The future potential for optimisation of MFPs, or design of similar systems with other starting points, is vast. For example, through high-throughput screening it is feasible to perform selection based on magnetic response, ESR response, or biological factors such as protein stability. Ultimately the development of these systems may lead to a new paradigm of quantum based tools for biological sensing, measurement, and actuation.

2 Optically Detected Magnetic and Resonant Field Effects in Fluorescent Living Cells

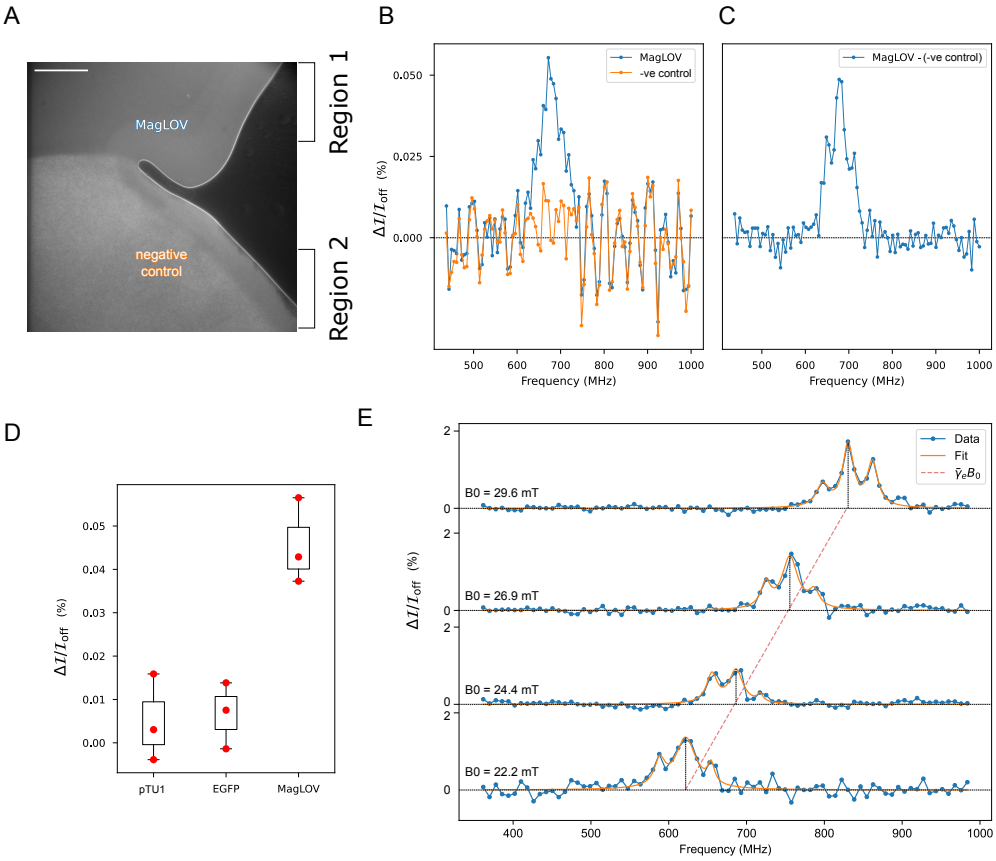

Fig. 2 Optically Detected Magnetic Resonance of MagLOV expressing *E. Coli.* To acquire an ODMR spectrum, a radio frequency is swept linearly with interleaved RF-on and RF-off periods, while the fluorescence is monitored under constant 450 nm excitation. **A.** Single field of view with MagLOV and negative control cells present as used in panels B/C. Scale bar is 100 µm. **B.** ODMR trace of bulk MagLOV cells and negative control cells in the same field of view, found by integrating horizontal regions 1 and 2 of panel A. **C.** Treating the negative control signal as reference (i.e. not carrying an ODMR signal, but carrying other signals due to resonant heating etc.) we subtract it from the MagLOV signal, yielding a sharp ODMR peak and hyperfine structure (side peaks). **D.** ODMR of bulk cells (MagLOV 2 R11 f) (similar to A, but only one type of cell), performed in biological triplicates at the same magnetic field $B_0 \approx 24.3\,\mathrm{mT}$ to compare peak ODMR contrast measured at the resonant frequency 680 MHz **E.** The static magnetic field B_0 was varied by adjusting the magnet's z-position, and ODMR spectra recorded. The red-dashed line is not a fit; it is a line drawn with slope equal to the electron gyromagnetic ratio.

Optically detected magnetic resonance (ODMR) (or reaction yield detected magnetic resonance, RYDMR) is both a diagnostic test for the existence of the proposed spin

correlated radical pair (discussed below) [13] and, due to its relative simplicity, an effective measurement modality for performing readout from quantum sensing devices for biological and materials applications [7, 8, 14–18]. In general, in the presence of an external static magnetic field B_0, ODMR involves the introduction of an oscillating magnetic field B_1, which is resonant with electron spin-flip transition energies. Driving these spin-flips changes the dynamics of the fluorophore excitation/emission photocycle, leading to a change in fluorescence on resonance. We observed a positive change in fluorescence for ODMR which, taken together with the negative change in fluorescence for the MFE, indicates a singlet-triplet system, in this case likely to be a spin correlated radical pair (SCRP) [3].

Previous studies reported MFEs arising from flavin interactions with protein backbones in terms of the SCRP mechanism [19–24]. Furthermore, radical pair intermediates are known to form in the LOV2 domain *Avena sativa* phototropin 1 (AsLOV2) variant $C_{450}A$ (the precursor protein to MagLOV) [25], as well as in related LOV domains [26–28]. The SCRP is a transient reaction intermediate, formed upon electron transfer from a donor to an acceptor molecule. The two unpaired spin-$\frac{1}{2}$ electrons couple to form a correlated pair with total electron spin angular momentum S of either 0 (singlet, $|S\rangle$) or 1 (triplet, $|T\rangle$) [Fig. 1 B]. Following creation of the radical pair either in the singlet or triplet state, interconversion can occur between the singlet and triplet states. At zero and low static magnetic fields B_0, mixing occurs rapidly and between all four states and is mediated by hyperfine interactions and relaxation. At higher fields, Zeeman splitting energetically isolates the $|T_\pm\rangle$ from $|T_0\rangle$, reducing singlet-triplet mixing to occur only between $|S\rangle$ and $|T_0\rangle$, which is the basis for MFEs. In general, this leads to a decrease in fluorescence if the initial radical pair was formed in the triplet state, which we conclude is the case based on our magnetic field effect experiments [Fig. 1 D]. With the introduction of an oscillating magnetic field B_1 on resonance with the $|T_0\rangle \leftrightarrow |T_\pm\rangle$ transitions, mixing between these states is enabled again [Fig. 1 A,B], leading to an increase in fluorescence as is observed in our ODMR experiments [Fig. 1 E]. The changes in fluorescence are due to the different recombination rates for singlet state and triplet state SCRPs. Only singlet SCRPs can recombine to the ground state via back electron transfer, but either state can go on to form uncorrelated radicals which recombine to the ground state. Therefore, by changing the population levels of the singlet and triplet radical pair states as described above, the rate of ground state replenishment is altered, leading to a detectable change in fluorescence.

We performed MFE and ODMR imaging using a widefield epifluorescence microscope (see S1.6). First, we measured the MagLOV MFE (see an example trace in Fig. 1 D), confirming that MagLOV exhibits a large MFE of $\Delta\mathcal{I}/\mathcal{I}_{\text{off,sat.}} = -30\%$. We then recorded an ODMR spectrum from MagLOV and compared with a negative control [Fig. 2 A], revealing an ODMR signal is present only when the MagLOV protein is expressed. In brief, samples were confined between two glass coverslips beneath a stripline antenna printed circuit board (PCB) (see S1.9). The antenna board was placed inverted on the microscope stage and a permanent magnet was fixed above,

applying a constant static field $B_0 \sim 25\,\mathrm{mT}$ in the z-direction, perpendicular to the RF modulation $B_1 \sim 0.3\,\mathrm{mT}$ field supplied by the stripline antenna. We grew *E. coli* expressing MagLOV, and *E. coli* transformed with the same plasmid devoid of the MagLOV protein coding sequence (negative control), scraped samples of each and placed cell conglomerates next to each other in the same field of view above the stripline [Fig. 2 A]. Integrating the brightness of the signal over the labelled regions of the image yields the MagLOV curve and negative control curves in [Fig. 2 B] (note that negative control cells are visible due to autofluorescence [29]). In the fluorescence signal from both cell types, we see non-magnetic resonance effects, hypothesised to arise from resonances inherent in the experimental hardware. However, the MagLOV protein fluorescence *also* exhibits an ODMR signal at the expected ESR frequency of $\omega_{RF} = \bar{\gamma}_e B_0 = 684\,\mathrm{MHz}$ for $B_0 = 24.4\,\mathrm{mT}$. Removing the resonant effects by subtracting the two signals [Fig. 2 C] reveals a three-peak hyperfine structure. Furthermore, we imaged cell conglomerates transformed with an empty plasmid (negative control), MagLOV plasmid (same as empty plus MagLOV), and an identical plasmid where MagLOV is replaced with EGFP [30] (which is much brighter than MagLOV) in biological triplicates, and only observed an ODMR resonance in cells expressing MagLOV [Fig. 2 D].

Next, we prepared a dilute sample in a buffer allowing us to isolate single cells. We recorded ODMR spectra at various B_0 fields by adjusting the z-position of the static magnet [Fig. 2 E]. The central ODMR resonance follows the expected ESR relationship $\omega_{RF} = \bar{\gamma}_e B_0$, confirming the RF field is driving spin transitions of a spin-$\frac{1}{2}$ electron [31, 32]. The signal-to-noise is significantly improved by averaging over many cells in a field of view, however, it is also possible to extract an ODMR signal from a single cell, with an ODMR contrast of 4 % [Fig. 1 E]. Given the number of proteins expressed is at most of order 10^5 per cell [33], this represents achieving sufficient signal-to-noise ratio with a reduction of at least 3 orders of magnitude in the number of spins required when compared to traditional ESR techniques under similarly ambient conditions [7]. On the other hand, the contrast appears to be reduced for bulk measurements (for example we saw an ODMR contrast of $\sim 0.05\%$ in Fig. 2 B) compared to single cells, likely because of increased background fluorescence, especially in the case of cell conglomerates.

3 Bound Flavin Radical Pair Model supported by MFE Spectroscopy and ODMR Measurements

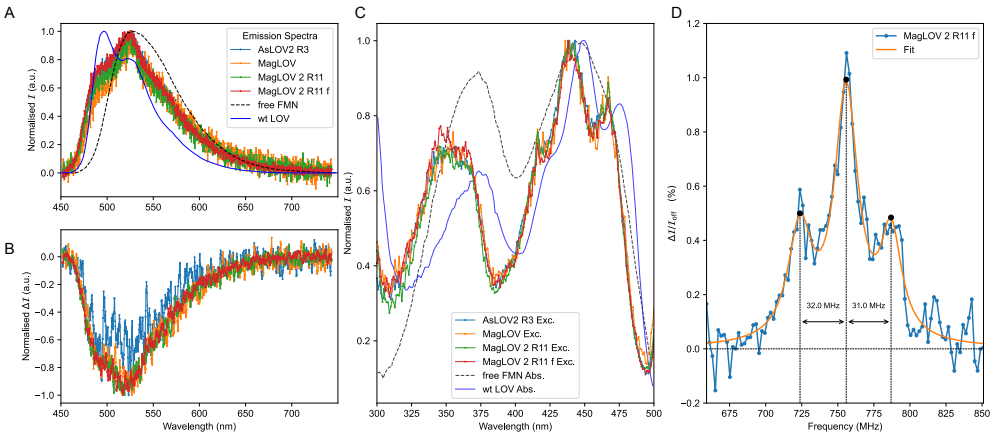

Fig. 3 Spectral, MFE and ODMR data supporting model of bound flavin Radical Pair. A. Emission spectra with 450 nm excitation acquired for bulk cell suspensions in PBS buffer. Emission spectra for free FMN and purified wt-LOV protein (440 nm exc.) are adapted from [34]. **B.** Wavelength dependence of magnetic field-induced modulation of emission intensity where $\Delta\mathcal{I} = \mathcal{I}(B_0 = 10\text{ mT}) - \mathcal{I}(B_0 = 0\text{ mT})$. Note that here we display the absolute difference as normalising by $\mathcal{I}(B_0 = 0\,\text{mT})$ obscures the wavelength dependence. **C.** Excitation spectra for 510 nm emission also acquired for bulk MagLOV cell suspensions in PBS buffer. Vibrational fine structure in the singlet energy transitions $S_0 \rightarrow S_1$ and $S_0 \rightarrow S_2$ (where S_n is the nth excited singlet state) bands $\sim$ 450 nm and $\sim$ 350 nm respectively indicates the emitting flavin is bound. Absorption spectra for Free FMN/wt-LOV adapted from [34]. **D.** ODMR recorded over a zoomed-in frequency band. The spectrum is structured, likely as a result of hyperfine couplings between one of the radicals and a nitrogen nucleus on the FMN co-factor.

Adopting the SCRP model prompts consideration of the electron donor and acceptor identities. Both previous studies, and our spectral data in Fig. 3, support identifying the acceptor molecule as the FMN cofactor [25, 27]. For all variants of MFPs expressed in cells, we find that the wavelength-resolved fluorescence intensity modulated by the applied magnetic field (ΔI) in [Fig 3 A, B] matches the FMN emission spectrum, supporting that both MFE and ODMR are detected on the flavin emission. The excitation spectrum shows vibrational fine structure [Fig 3 C] and is in excellent agreement with the dark-state absorption spectrum of AsLOV2 C_{450}A [35], confirming the emission originates from *bound* FMN, i.e. the observed MFEs are not a result of cellular autofluorescence as has been reported for similar systems [36, 37]. The ODMR data further supports identifying the FMN as the acceptor, as the hyperfine resonances (side peaks) are spaced at $\pm 31\,\text{MHz}$ from the central peak [Fig. 3 D], in agreement with the anisotropic coupling $A_z = 31.7(20)\,\text{MHz}$ to the flavin ^{14}N(10) nucleus reported by Weber et al. [38].

Regarding the donor molecule, for AsLOV2 $C_{450}A$, single point mutations leading to quenching of the emissive NMR signal suggest W_{491} as the electron donor [39], which was corroborated by isotopic labelling of Trp residues in AsLOV2 $C_{450}A$ [40]. However, given the extent of mutations in the variants studied here, we cannot confirm W_{491} is still the counter-radical. In the structurally related iLOV-Q489, derived from *A. thaliana* phototropin-2 (AtPhot2) LOV2 domain, transient absorption spectra revealed a neutral tryptophan radical, $Trp^{\bullet}$, is formed in conjunction with $FMNH^{\bullet}$, and photoinduced flavin reduction in single-point mutations of selected tyrosine and tryptophan residues suggested several amino acids that might be involved in SCRP formation [41].

4 Magnetic Field Effect can be Engineered by Directed Evolution

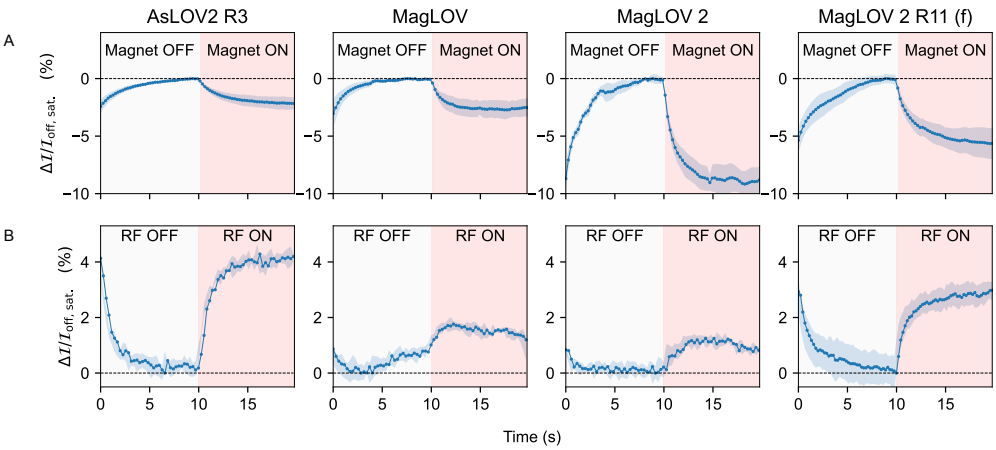

Fig. 4 MFE and ODMR Dynamics of Engineered Variants. A. MFP variants were engineered by mutagenesis and directed evolution; from rounds R3 to R10 selection was performed to increase the MFE at saturation, while MagLOV 2 R11 f was selected for increased rate of MFE prior to saturation. In these measurements a magnetic field of $B_0 = 10$ mT was switched on and off with a period of 20 s. The traces shown are the average (and standard deviation) over multiple periods. **B.** The equivalent to an MFE experiment was performed using ODMR on resonance, with a static field of $B_0 = 29.9$ mT and corresponding resonant field B_1 frequency of $\omega_{RF} = 754$ MHz switched on and off with a 20 s period, averaged as above.

The AsLOV2 domain has been widely used as a starting point for engineering optogenetic and other light-dependent protein functionalities [42, 43]. For MFPs, depending on the application, one could choose to optimise for metrics including MFE magnitude, saturation rate, ODMR contrast, ODMR saturation rate, ODMR line-width broadening, hyperfine couplings, and others; we here demonstrate this potential by selecting for MFE saturation rate. As previously reported [1], starting from ancestor variant AsLOV2 $C_{450}A$ [44] we used directed evolution to create variants of MFPs

including MagLOV. This engineering process (S1.3) involved successive rounds of mutagenesis (introducing all single amino-acid changes to a given variant), followed by screening of samples from this variant library to select for increased MFE magnitude. Here, using the same methodology, we further engineered MagLOV 2, and by selecting for maximisation of saturation rate (rather than magnitude) of MFE, MagLOV 2 R11 f, demonstrating the possibility to perform selection based on different aspects of the MFE. Visually distinguishing between the MFE rates of variants is best observed in data taken from bulk solutions [SI Fig. S5 A], which is averaged over many more cells and less prone to distortion by background subtraction. The observed changes in MFE [Fig. 4 A and SI Fig. S5 A] can be interpreted based on past work investigating flavin magnetic field-sensitive photochemistry: The MFE enhancement kinetics (i.e. time to MFE saturation) are determined by the ratio between the rates that donor and acceptor free radicals return to ground state [45]. As such we hypothesise the change in MFE enhancement timescale reflects an asymmetric change in the degree of solvent exposure of the radical entities, altering the aforementioned ratio. For instance, with the mutations introduced in MagLOV 2 R11 f, the acceptor return rate increases relatively to the donor, decreasing the time constant of the response. Interestingly, the ODMR contrast and rates are changed, but not necessarily in simple correlation with MFE contrast [Fig. 4 B]. This raises the possibility of engineering orthogonal fluorescent signatures, expanding again the number of tags available for multiplexing (for instance with further engineering the total might be #emission colors $\times$ #MFE signatures $\times$ #ODMR signatures). Alternatively, if ODMR contrast and MFE magnitude are not independent, then MFE could be used as a proxy for improved ODMR, since the simplicity of measuring MFE makes it better suited to directed evolution experiments, while certain applications (such as measurements of reporter spatial localisation) are better suited to ODMR.

5 Demonstration of Multiplexing and Signal Lock-in

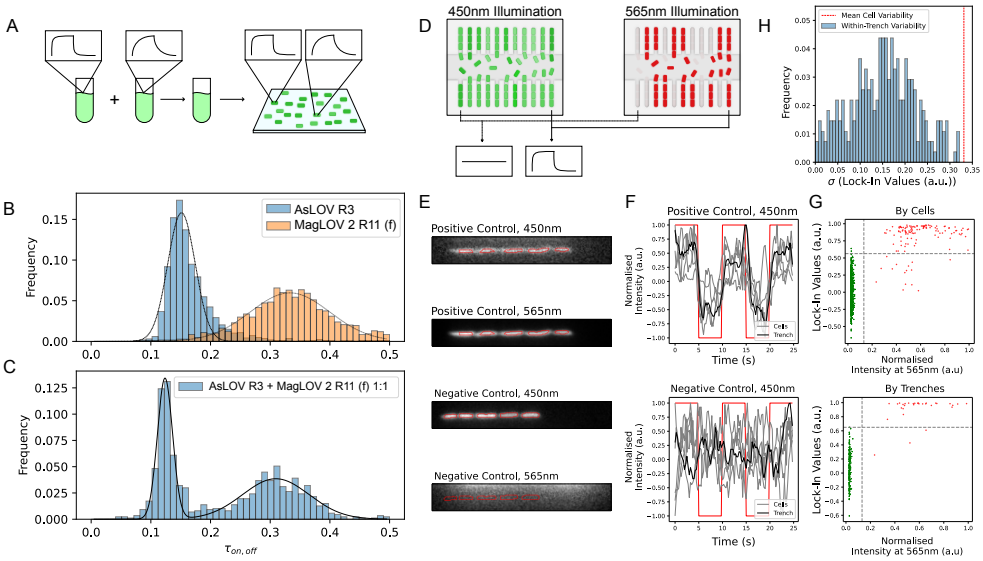

Fig. 5 Multiplexing and Lock-in Applications using MFE. A. Illustration of the preparation of multiple variants on a coverslip. **B, C.** Exponential curves were fit to the MFE of each cell in each field of view. In B, the separate populations are shown, illustrating MagLOV 2 R11 f has a greater exponential parameter $\tau_{on,off}$, and that overlaying the two populations produces a bi-modal distribution with small overlap (S1.11.1). **C.** A two-Gaussian function is fit to the bi-modal distribution of a sample with $1:1$ mixture of the variants. The ratio of areas under the Gaussians is AsLOV2 R3 : MagLOV 2 R11 f $= 0.82 : 1$, consistent with $0.92 : 1$ found from the area under the Gaussian fits in B. **D.** Schematic illustration of the microfluidic setup. Cells expressing either MagLOV and EGFP fluoresce green under 450 nm illumination, whereas only cells expressing MagLOV are visible under 565 nm illumination, since they co-express mCherry. The chip is composed of two rows of trenches (vertical lines) connected by a channel bringing fresh media into the system and carrying old cells out. **E.** Cropped view of single trenches, with cells circled in red as identified by a cell-segmentation algorithm (S1.12). **F.** Time-series of the 450 nm illumination fluorescence response for the individual cells depicted in E over time, as a magnetic field $B_0 = 10$ mT is switched on and off (red line). Both the traces for each cell in the trench (grey lines), and the average trace over all the cells in the trench (black line) are shown. **G.** Confusion scatter plot for classifying whether cells express MagLOV or EGFP based on magnetic response, taking the 565 nm fluorescence as ground-truth and using the lock-in value (S1.12) as the predictor. Top left quadrant are false negatives, top right quadrant are true positives, bottom left quadrant are true negatives, and bottom right quadrant are false positives. The balanced accuracy by cells and by trenches is 0.99, see S2.1 for classification data. **H.** The standard deviation σ of the lock-in values in G is calculated between cells in each trench (blue histogram) and between all cells in all trenches (mean value in red dashed line).

Our library of MFP variants exhibits differences in the rate and magnitude of response across both MFE and ODMR characterisation. Where such differences can be engineered orthogonally between variants, they open the possibility of using libraries of MFP reporters as a multiplexing tool to extract several signals from

a single measurement (i.e. fluorescence intensity in a single wavelength band). To demonstrate this potential in fluorescence microscopy, we created equal mixtures of AsLOV2 R3 and MagLOV 2 R11 f and measured single-cell MFEs across the combined sample [Fig. 5 A]. We initially characterised each variant in isolation, measuring fluorescence traces for ~ 500 cells in a field of view, and exponential rise/fall functions (characterised by an amplitude A and rate parameter B) were fit to periods with electromagnet off/on respectively, which allows estimation of intrapopulation variability [Fig. 5 B]. We then characterised a mixture of these variants [Fig. 5 C], for which parameter values fit to single cells show strong bi-modality, enabling the population to be decomposed into sub-populations identified by which magneto-sensitive fluorescent variant is expressed. Separation of sub-populations is more challenging for variants with similar dynamics, or when attempting separation based on MFE amplitude (A) which we hypothesise is confounded by factors including intracellular variability in protein expression and environment.

Using a microfluidics setup, we further investigated the intracellular variability of variants of MFPs, and demonstrate the possibility of lock-in detection in weak signal environments. Cells expressing EGFP [30] and co-expressing mCherry [46] and MagLOV were mixed and loaded into a microfluidic "mother machine" chip consisting of evenly spaced trenches, which after a few hours growth are each filled only with cells whose ancestor is the cell at the closed end of the trench (i.e. they may be considered clonal) [Fig. 5 D]. The cells were imaged using the same widefield fluorescence microscopy setup as described previously. Using MFE-based lock-in detection, we found that MagLOV cells could be identified distinctly from EGFP in most cases (using mCherry as a ground truth), with accuracy improving when averaging over a trench compared to distinguishing single cells [Fig. 5 E-G]. This approach allows variability to be attributed to inter-clonal or intra-clonal sources; we observe that mean intra-trench variability (quantified by standard deviation over 5-8 cells in the trench) is approximately half that of the variability over all MagLOV-positive cells [Fig. 5 H]. This suggests approximately one third of the total arises from intra-clonal noise sources (e.g. phenotypic variability over 3-4 generations, camera and accompanying measurement noise), with inter-clonal sources (longer term phenotypic variability, variation in local environment) contributing the remainder.

6 Discussion

Directed evolution, enabled by straightforward fluorescence screening, has proved to be a powerful technique to engineer proteins exhibiting magneto-sensitive responses. The advent of stable, highly responsive magneto-sensitive proteins represents a paradigm shift; transitioning from systems studied primarily for scientific interest toward engineerable tools with potential for widespread application. Previously existing natural and engineered proteins (typically designed as model representatives of the cryptochrome) exhibited comparatively small responses to magnetic fields, required sophisticated experimental apparatus for study, did not exhibit MFEs in

living cells, were prone to rapid light-induced degradation, and were therefore unsuitable for biotechnological applications or high-throughput setups required for directed evolution [23, 47, 48]. That said, compared with other candidates for quantum biological sensing, two unique advantages of a protein-based system are (a) that it is configurable: significant engineering improvements can be made (relatively simply) by changing the DNA encoding the protein, and that (b) that it can be endogenously expressed, opening the door to genetically engineered regulation of expression. MFPs therefore are the best of both worlds, enabling robust quantum measurements while also being highly amenable to engineering and cellular integration.

While the properties of the MFPs we generated (photostability, MFE magnitude) are far superior to previous proteins exhibiting MFEs, their optimisation is by no means complete. Similarly, there remains significant opportunity for mechanistic investigations utilising the wide array of techniques previously applied to biological systems exhibiting MFEs and ESR [26, 43, 48–51]. Building such mechanistic understanding would support use of rational design methods to develop biotechnological tools. Crucially, understanding the mechanism of action and high throughput screening (similar to and more advanced than we demonstrate here) can go hand in hand - for instance by identifying a proxy property of MFE to optimise to achieve a desired ODMR property in application. In general, precisely which metric(s) are chosen for optimisation depends on the application in mind, be it utilising MFE or ODMR, or favouring magnitude or speed of response as was of interest for the lock-in and multiplexing applications we demonstrated. As such - much like fluorescent proteins - we expect MFPs will also be engineered to make general improvements, such as to solubility, photo-stability and quantum-yield [52]. Finally, we hope that the development of MFPs can serve as the starting point for magnetically controlled biological actuators, whereby application of a local magnetic field can have downstream cellular effects - such a technology would be of significant biomedical and biotechnological interest.

Supplementary information.

- `SI.pdf`
- `CalibrationData.xlsx`
- `primers.fasta`

Acknowledgements. The authors would like to thank Kevin Henbest for helpful discussions, and Islay Robertson and Phillip Reineck for assistance with proof of concept experiments.
The protein structure in Fig. 1 was rendered using ChimeraX [53].
The EcoFlex kit was a gift from Paul Freemont (Addgene kit #1000000080) [54].

Declarations

GA and SS were supported by funding from the Biotechnology and Biological Sciences Research Council (UKRI-BBSRC) [grant number BB/T008784/1]. JJ and VTF were supported by funding from the Engineering and Physical Sciences Research Council

(UKRI-EPSRC) [grant number EP/W524311/1]. IK is supported in part by the Engineering and Physical Sciences Research Council under the EEBio Programme Grant, EP/Y014073/1. HS recognises support from the Philip Leverhulme Prize.

Author contribution.

- Gabriel Abrahams - conceptualisation, development of ODMR setup, development of widefield MFE setup, experimental measurements, analysis, interpretation
- Vincent Spreng - sample preparation, widefield MFE measurements, cloning plasmids and strains (post directed evolution) strategy and execution
- Ana Stuhec - spectral measurements, bulk MFE measurements, analysis, interpretation
- Idris Kempf - microscope platform development, performing microfluidics experiments, analysis for microfluidics experiments
- Jessica James - microscope platform development, carried out performing microfluidics experiments, analysis for microfluidics experiments
- Kirill Sechkar - microfluidics platform development, performing microfluidics experiments
- Scott Stacey - cloning plasmids and strains (post directed evolution) strategy and execution, figure preparation
- Vicente Trelles-Fernandez - cloning plasmids and strains (post directed evolution) strategy and execution
- Lewis M. Antill - analysis, interpretation
- Maria Ingaramo - variant generation by directed evolution
- Andrew York - conceptualisation of MFE experiment, project co-ordination
- Jean-Philippe Tetienne - preliminary experiments, analysis
- Christiane R. Timmel - project co-ordination, analysis, supervision
- Harrison Steel - project co-ordination and conceptualisation, development of microscopy setup, supervision

References

[1] Hayward, R.F., Lazzari-Dean, J.R., York, A.G., Ingaramo, M.: GFP Magnetofluorescence. https://doi.org/10.5281/zenodo.8137174 Accessed 2023-10-30

[2] Halavaty, A.S., Moffat, K.: N- and C-Terminal Flanking Regions Modulate Light-Induced Signal Transduction in the LOV2 Domain of the Blue Light Sensor Phototropin 1 from Avena sativa, **46**(49), 14001–14009 https://doi.org/10.1021/bi701543e . Accessed 2024-11-01

[3] Timmel, C.R., Henbest, K.B.: A Study of Spin Chemistry in Weak Magnetic Fields **362**(1825), 2573–2589 4142313. Accessed 2024-10-21

[4] Finkler, A., Dasari, D.: Quantum Sensing and Control of Spin-State Dynamics in the Radical-Pair Mechanism **15**(3), 034066 https://doi.org/10.1103/PhysRevApplied.15.034066 . Accessed 2024-10-31

[5] Sukumar, U.K., Natarajan, A., Massoud, T.F., Paulmurugan, R.: Applications of fluorescent protein-based sensors in bioimaging. In: Cheng, Z. (ed.) Fluorescent Imaging in Medicinal Chemistry, pp. 149–183. Springer. https://doi.org/10.1007/7355_2019_90 . https://doi.org/10.1007/7355_2019_90 Accessed 2024-10-26

[6] Crone, D.E., Huang, Y.-M., Pitman, D.J., Schenkelberg, C., Fraser, K., Macari, S., Bystroff, C., Crone, D.E., Huang, Y.-M., Pitman, D.J., Schenkelberg, C., Fraser, K., Macari, S., Bystroff, C.: GFP-Based Biosensors. In: State of the Art in Biosensors - General Aspects. IntechOpen. https://doi.org/10.5772/52250 . https://www.intechopen.com/chapters/43428 Accessed 2024-10-26

[7] Simpson, D.A.: Quantum probes for biology: Unlocking single molecule dynamics **24**, 7–9 https://doi.org/10.1016/j.nantod.2018.12.001 . Accessed 2024-10-21

[8] Segawa, T.F., Igarashi, R.: Nanoscale quantum sensing with Nitrogen-Vacancy centers in nanodiamonds – A magnetic resonance perspective **134–135**, 20–38 https://doi.org/10.1016/j.pnmrs.2022.12.001 . Accessed 2024-10-25

[9] Moore, T.A., Kwiram, A.L.: Investigation of the triplet state of flavines and flavoproteins by optical detection of magnetic resonance **13**(26), 5403–5407 https://doi.org/10.1021/bi00723a025 . Accessed 2024-11-10

[10] Moehl, K.W., Lous, E.J., Hoff, A.J.: Low-power, low-field RYDMAR of the primary radical pair in photosynthesis **121**(1), 22–27 https://doi.org/10.1016/0009-2614(85)87147-5 . Accessed 2024-10-23

[11] Braun, T., Drescher, M., Summerer, D.: Expanding the Genetic Code for Site-Directed Spin-Labeling **20**(2), 373 https://doi.org/10.3390/ijms20020373 30654584. Accessed 2024-10-26

[12] Matysik, J., Gerhards, L., Theiss, T., Timmermann, L., Kurle-Tucholski, P., Musabirova, G., Qin, R., Ortmann, F., Solov'yov, I.A., Gulder, T.: Spin Dynamics of Flavoproteins **24**(9), 8218 https://doi.org/10.3390/ijms24098218 . Accessed 2024-10-21

[13] Henbest, K.B., Kukura, P., Rodgers, C.T., Hore, P.J., Timmel, C.R.: Radio Frequency Magnetic Field Effects on a Radical Recombination Reaction: A Diagnostic Test for the Radical Pair Mechanism **126**(26), 8102–8103 https://doi.org/10.1021/ja048220q . Accessed 2024-10-21

[14] Scholten, S.C., Healey, A.J., Robertson, I.O., Abrahams, G.J., Broadway, D.A., Tetienne, J.-P.: Widefield quantum microscopy with nitrogen-vacancy centers in diamond: Strengths, limitations, and prospects **130**(15), 150902 https://doi.org/10.1063/5.0066733 . Accessed 2024-10-25

[15] Levine, E.V., Turner, M.J., Kehayias, P., Hart, C.A., Langellier, N., Trubko, R., Glenn, D.R., Fu, R.R., Walsworth, R.L.: Principles and techniques of

the quantum diamond microscope **8**(11), 1945–1973 https://doi.org/10.1515/nanoph-2019-0209 . Accessed 2024-10-25

[16] Aslam, N., Zhou, H., Urbach, E.K., Turner, M.J., Walsworth, R.L., Lukin, M.D., Park, H.: Quantum sensors for biomedical applications **5**(3), 157–169 https://doi.org/10.1038/s42254-023-00558-3 . Accessed 2024-10-25

[17] Ishiwata, H., Watanabe, H.C., Hanashima, S., Iwasaki, T., Hatano, M.: Label-Free Phase Change Detection of Lipid Bilayers Using Nanoscale Diamond Magnetometry **4**(4), 2000106 https://doi.org/10.1002/qute.202000106 . Accessed 2024-10-25

[18] McCloskey, D.J., Dontschuk, N., Stacey, A., Pattinson, C., Nadarajah, A., Hall, L.T., Hollenberg, L.C.L., Prawer, S., Simpson, D.A.: A diamond voltage imaging microscope **16**(10), 730–736 https://doi.org/10.1038/s41566-022-01064-1 . Accessed 2024-10-25

[19] Antill, L.M., Woodward, J.R.: Flavin Adenine Dinucleotide Photochemistry Is Magnetic Field Sensitive at Physiological pH **9**(10), 2691–2696 https://doi.org/10.1021/acs.jpclett.8b01088 . Accessed 2024-05-28

[20] Antill, L.M., Beardmore, J.P., Woodward, J.R.: Time-resolved optical absorption microspectroscopy of magnetic field sensitive flavin photochemistry **89**(2), 023707 https://doi.org/10.1063/1.5011693 . Accessed 2024-10-30

[21] Dodson, C.A., Wedge, C.J., Murakami, M., Maeda, K., Wallace, M.I., Hore, P.J.: Fluorescence-detected magnetic field effects on radical pair reactions from femtolitre volumes **51**(38), 8023–8026 https://doi.org/10.1039/C5CC01099C . Accessed 2024-10-30

[22] Evans, E.W., Li, J., Storey, J.G., Maeda, K., Henbest, K.B., Dodson, C.A., Hore, P.J., Mackenzie, S.R., Timmel, C.R.: Sensitive fluorescence-based detection of magnetic field effects in photoreactions of flavins **17**(28), 18456–18463 https://doi.org/10.1039/C5CP00723B . Accessed 2023-08-02

[23] Bialas, C., Barnard, D.T., Auman, D.B., McBride, R.A., Jarocha, L.E., Hore, P.J., Dutton, P.L., Stanley, R.J., Moser, C.C.: Ultrafast flavin/tryptophan radical pair kinetics in a magnetically sensitive artificial protein **21**(25), 13453 https://doi.org/10.1039/c9cp01916b 31187821. Accessed 2024-10-30

[24] Antill, L.M., Takizawa, S.-y., Murata, S., Woodward, J.R.: Photoinduced flavin-tryptophan electron transfer across vesicle membranes generates magnetic field sensitive radical pairs **117**(19), 2594–2603 https://doi.org/10.1080/00268976.2018.1524525 . Accessed 2024-10-30

[25] Richter, G., Weber, S., Römisch, W., Bacher, A., Fischer, M., Eisenreich, W.: Photochemically Induced Dynamic Nuclear Polarization in a C450A Mutant of

the LOV2 Domain of the Avena sativa Blue-Light Receptor Phototropin **127**(49), 17245–17252 https://doi.org/10.1021/ja053785n . Accessed 2024-11-01

[26] Schleicher, E., Kowalczyk, R.M., Kay, C.W.M., Hegemann, P., Bacher, A., Fischer, M., Bittl, R., Richter, G., Weber, S.: On the Reaction Mechanism of Adduct Formation in LOV Domains of the Plant Blue-Light Receptor Phototropin **126**(35), 11067–11076 https://doi.org/10.1021/ja049553q . Accessed 2024-10-19

[27] Kothe, G., Lukaschek, M., Link, G., Kacprzak, S., Illarionov, B., Fischer, M., Eisenreich, W., Bacher, A., Weber, S.: Detecting a new source for photochemically induced dynamic nuclear polarization in the LOV2 domain of phototropin by magnetic-field dependent (13)C NMR spectroscopy **118**(40), 11622–11632 https://doi.org/10.1021/jp507134y 25207844

[28] Brosi, R., Illarionov, B., Heidinger, L., Kim, R.-R., Fischer, M., Weber, S., Bacher, A., Bittl, R., Schleicher, E.: Coupled Methyl Group Rotation in FMN Radicals Revealed by Selective Deuterium Labeling, 9–11331 https://doi.org/10.1021/acs.jpcb.9b11331 . Accessed 2024-10-19

[29] Surre, J., Saint-Ruf, C., Collin, V., Orenga, S., Ramjeet, M., Matic, I.: Strong increase in the autofluorescence of cells signals struggle for survival **8**(1), 12088 https://doi.org/10.1038/s41598-018-30623-2 . Accessed 2024-11-20

[30] Cormack, B.P., Valdivia, R.H., Falkow, S.: FACS-optimized mutants of the green fluorescent protein (GFP) **173**(1), 33–38 https://doi.org/10.1016/0378-1119(95)00685-0 . Accessed 2024-02-05

[31] Wedge, C.J., Lau, J.C.S., Ferguson, K.-A., Norman, S.A., Hore, P.J., Timmel, C.R.: Spin-locking in low-frequency reaction yield detected magnetic resonance **15**(38), 16043–16053 https://doi.org/10.1039/C3CP52019F . Accessed 2024-10-31

[32] Fan, X., Myers, T.G., Sukra, B.A.D., Gabrielse, G.: Measurement of the Electron Magnetic Moment **130**(7), 071801 https://doi.org/10.1103/PhysRevLett.130.071801 . Accessed 2024-10-30

[33] Dolgalev, G.V., Safonov, T.A., Arzumanian, V.A., Kiseleva, O.I., Poverennaya, E.V.: Estimating Total Quantitative Protein Content in Escherichia coli, Saccharomyces cerevisiae, and HeLa Cells **24**(3), 2081 https://doi.org/10.3390/ijms24032081 36768409. Accessed 2024-10-24

[34] Gregor, C., Sidenstein, S.C., Andresen, M., Sahl, S.J., Danzl, J.G., Hell, S.W.: Novel reversibly switchable fluorescent proteins for RESOLFT and STED nanoscopy engineered from the bacterial photoreceptor YtvA **8**(1), 2724 https://doi.org/10.1038/s41598-018-19947-1 . Accessed 2024-11-06

[35] Kay, C.W.M., Schleicher, E., Kuppig, A., Hofner, H., Rüdiger, W., Schleicher,

M., Fischer, M., Bacher, A., Weber, S., Richter, G.: Blue Light Perception in Plants: DETECTION AND CHARACTERIZATION OF A LIGHT-INDUCED NEUTRAL FLAVIN RADICAL IN A C450A MUTANT OF PHOTOTROPIN * **278**(13), 10973–10982 https://doi.org/10.1074/jbc.M20550920012525505. Accessed 2024-10-19

[36] Ikeya, N., Woodward, J.R.: Cellular autofluorescence is magnetic field sensitive **118**(3), 2018043118 https://doi.org/10.1073/pnas.2018043118 . Accessed 2024-10-24

[37] Uzhytchak, M., Smolková, B., Frtús, A., Stupakov, A., Lunova, M., Scollo, F., Hof, M., Jurkiewicz, P., Sullivan, G.J., Dejneka, A., Lunov, O.: Sensitivity of endogenous autofluorescence in HeLa cells to the application of external magnetic fields **13**(1), 10818 https://doi.org/10.1038/s41598-023-38015-x . Accessed 2024-10-24

[38] Weber, S., Kay, C.W.M., Bacher, A., Richter, G., Bittl, R.: Probing the N(5) H Bond of the Isoalloxazine Moiety of Flavin Radicals by X- and W-Band Pulsed Electron–Nuclear Double Resonance **6**(2), 292–299 https://doi.org/10.1002/cphc.200400377 . Accessed 2024-10-19

[39] Eisenreich, W., Joshi, M., Weber, S., Bacher, A., Fischer, M.: Natural Abundance Solution 13C NMR Studies of a Phototropin with Photoinduced Polarization **130**(41), 13544–13545 https://doi.org/10.1021/ja805856r . Accessed 2024-11-01

[40] Eisenreich, W., Fischer, M., Römisch-Margl, W., Joshi, M., Richter, G., Bacher, A., Weber, S.: Tryptophan 13C nuclear-spin polarization generated by intraprotein electron transfer in a LOV2 domain of the blue-light receptor phototropin **37**(2), 382–386 https://doi.org/10.1042/BST0370382 . Accessed 2024-11-01

[41] Kopka, B., Magerl, K., Savitsky, A., Davari, M.D., Röllen, K., Bocola, M., Dick, B., Schwaneberg, U., Jaeger, K.-E., Krauss, U.: Electron transfer pathways in a light, oxygen, voltage (LOV) protein devoid of the photoactive cysteine **7**(1), 13346 https://doi.org/10.1038/s41598-017-13420-1 . Accessed 2024-10-27

[42] Lungu, O.I., Hallett, R.A., Choi, E.J., Aiken, M.J., Hahn, K.M., Kuhlman, B.: Designing Photoswitchable Peptides Using the AsLOV2 Domain **19**(4), 507–517 https://doi.org/10.1016/j.chembiol.2012.02.006 . Accessed 2023-08-02

[43] Maity, S., Price, B.D., Wilson, C.B., Mukherjee, A., Starck, M., Parker, D., Wilson, M.Z., Lovett, J.E., Han, S., Sherwin, M.S.: Triggered Functional Dynamics of AsLOV2 by Time-Resolved Electron Paramagnetic Resonance at High Magnetic Fields **62**(13), 202212832 https://doi.org/10.1002/anie.202212832 . Accessed 2024-10-19

[44] Petrenčáková, M., Varhač, R., Kožár, T., Nemergut, M., Jancura, D., Schwer, M.-S., Sedlák, E.: Conformational properties of LOV2 domain and its C450A variant

within broad pH region **259**, 106337 https://doi.org/10.1016/j.bpc.2020.106337 . Accessed 2024-10-19

[45] Kattnig, D.R., Evans, E.W., Déjean, V., Dodson, C.A., Wallace, M.I., Mackenzie, S.R., Timmel, C.R., Hore, P.J.: Chemical amplification of magnetic field effects relevant to avian magnetoreception **8**(4), 384–391 https://doi.org/10.1038/nchem.2447 . Accessed 2024-02-01

[46] Shaner, N.C., Campbell, R.E., Steinbach, P.A., Giepmans, B.N.G., Palmer, A.E., Tsien, R.Y.: Improved monomeric red, orange and yellow fluorescent proteins derived from Discosoma sp. red fluorescent protein **22**(12), 1567–1572 https://doi.org/10.1038/nbt1037 . Accessed 2024-11-01

[47] Bialas, C., Jarocha, L.E., Henbest, K.B., Zollitsch, T.M., Kodali, G., Timmel, C.R., Mackenzie, S.R., Dutton, P.L., Moser, C.C., Hore, P.J.: Engineering an Artificial Flavoprotein Magnetosensor **138**(51), 16584–16587 https://doi.org/10.1021/jacs.6b09682 27958724. Accessed 2023-08-02

[48] Evans, E.W., Dodson, C.A., Maeda, K., Biskup, T., Wedge, C.J., Timmel, C.R.: Magnetic field effects in flavoproteins and related systems **3**(5), 20130037 https://doi.org/10.1098/rsfs.2013.0037 . Accessed 2023-08-02

[49] Brosi, R., Illarionov, B., Mathes, T., Fischer, M., Joshi, M., Bacher, A., Hegemann, P., Bittl, R., Weber, S., Schleicher, E.: Hindered Rotation of a Cofactor Methyl Group as a Probe for Protein-Cofactor Interaction **132**(26), 8935–8944 https://doi.org/10.1021/ja910681z . Accessed 2024-10-19

[50] Déjean, V., Konowalczyk, M., Gravell, J., Golesworthy, M.J., Gunn, C., Pompe, N., Elst, O.F.V., Tan, K.-J., Oxborrow, M., Aarts, D.G.A.L., Mackenzie, S.R., Timmel, C.R.: Detection of magnetic field effects by confocal microscopy **11**(30), 7772–7781 https://doi.org/10.1039/D0SC01986K . Accessed 2024-01-23

[51] Hore, P.J., Mouritsen, H.: The Radical-Pair Mechanism of Magnetoreception **45**(1), 299–344 https://doi.org/10.1146/annurev-biophys-032116-094545 27216936. Accessed 2023-08-10

[52] Gest, A.M.M., Sahan, A.Z., Zhong, Y., Lin, W., Mehta, S., Zhang, J.: Molecular Spies in Action: Genetically Encoded Fluorescent Biosensors Light up Cellular Signals https://doi.org/10.1021/acs.chemrev.4c00293 . Accessed 2024-11-15

[53] Meng, E.C., Goddard, T.D., Pettersen, E.F., Couch, G.S., Pearson, Z.J., Morris, J.H., Ferrin, T.E.: UCSF ChimeraX: Tools for structure building and analysis **32**(11), 4792 https://doi.org/10.1002/pro.4792 . Accessed 2024-10-20

[54] Moore, S.J., Lai, H.-E., Kelwick, R.J.R., Chee, S.M., Bell, D.J., Polizzi, K.M., Freemont, P.S.: EcoFlex: A Multifunctional MoClo Kit for E. coli Synthetic Biology **5**(10), 1059–1069 https://doi.org/10.1021/acssynbio.6b00031 27096716